analytical chemistry

Article

Cite This: Anal. Chem. 2019, 91, 14085−14092

pubs.acs.org/ac

# Aptamer Induced Multicolored AuNCs-$WS_2$ "Turn on" FRET Nano Platform for Dual-Color Simultaneous Detection of Aflatoxin$B_1$ and Zearalenone

Imran Mahmood Khan,[†,‡,∥,⊥] Sobia Niazi,[†,‡,∥,⊥] Ye Yu,[#] Ali Mohsin,[§] Bilal Sajid Mushtaq,[†,‡] Muhammad Waheed Iqbal,[†,‡] Abdur Rehman,[†,‡] Wasim Akhtar,[†,‡] and Zhouping Wang*[,†,‡,⊥,∥]

[†]State Key Laboratory of Food Science and Technology, Jiangnan University, Wuxi, 214122, China

[‡]School of Food Science and Technology, Jiangnan University, Wuxi, 214122, China

[§]East China University of Science and Technology, Shanghai, 200000, China

[⊥]International Joint Laboratory on Food Safety, Jiangnan University, Wuxi, 214122, China

[∥]Synergetic Innovation Center of Food Safety and Quality Control of Jiangsu Province, Wuxi 214122, China

[#]Technology Center of Zhangjiagang Entry-Exit Inspection and Quarantine Bureau, Zhangjiagang, 214114, China

Supporting Information

**ABSTRACT:** Mycotoxins posit serious threats to human and animal health, and numerous efforts have been performed to detect the multiple toxins by a single diagnostic approach. To best of our knowledge, for the first time, we synthesized an aptamer induced "turn on" fluorescence resonance energy transfer (FRET) biosensor using dual-color gold nanoclusters (AuNCs), L-proline, and BSA synthesized AuNCs (Lp-AuNCs and BSA-AuNCs), with $WS_2$ nanosheet for simultaneous recognition of aflatoxin$B_1$ ($AFB_1$) and zearalenone (ZEN) by single excitation. Here, $AFB_1$ aptamer stabilized blue-emitting AuNCs ($AFB_1$-apt-Lp-AuNCs) (at 442 nm) and ZEN aptamer functionalized with red-colored AuNCs (ZEN-apt-BSA-AuNCs) (at 650 nm) were employed as an energy donor and $WS_2$ nanosheet as a fluorescence quencher. With the addition of $AFB_1$ and ZEN, the change in fluorescence intensity (F.I) was recorded at 442 and 650 nm and can be used for simultaneous recognition with a detection limit of 0.34 pg $mL^{-1}$ ($R^2$ = 0.9931) and 0.53 pg $mL^{-1}$ ($R^2$ = 0.9934), respectively. Most importantly, the semiquantitative determination of $AFB_1$ and ZEN can also be realized through photovisualization. The current approach paves a new way to develop sensitive, selective, and convenient metal nanocluster-based fluorescent "switch-on" probes with potential applications in multipurpose biosensing.

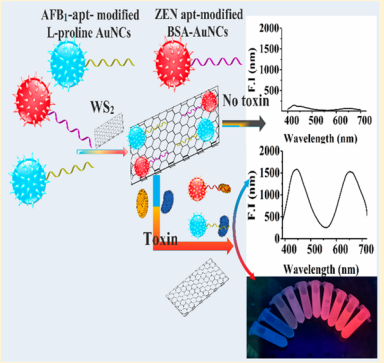




Food safety has incited as a grand global concern, impacting animal and human health along with feedstuff and also international trade and the food industry.[1−3] Among various uncertainty, mycotoxins are the foremost food safety concerns, causing foodborne illness and intoxication.[4,5] The health prospects stemming from mycotoxins may come from their toxicity, in particular, their mutagenic and carcinogenicity properties.[6] Although 400 common mycotoxins have been recognized, only a few of them have significance related to human health.[6,7] Among them, $AFB_1$ and ZEN, one of the major challenging food concerns, have strong carcinogenic consequences. $AFB_1$ is the most toxic and prevalent mycotoxin, which is enumerated as a group I carcinogen by the International Agency for Research on Cancer (IARC) due to their growth retardation, mutagenic potential, and carcinogenic tendencies.[8] ZEN is also one of the most imperative, nonsteroidal estrogenic *Fusarium* mycotoxins, and it has been categorized as a group III carcinogen.[9]

Mostly, fungi are adopted to produce multiple mycotoxins simultaneously and can contaminate feed and foodstuff at the same time.[10,11] This is primarily significant regarding $AFB_1$ and ZEN, which are omnipresent and co-occur in a range of maize and maize products.[12] Therefore, it is important to detect these toxins to prevent damage in humans and to eradicate them from corn and other agricultural foodstuffs.

To resolve the food safety dilemma, multiple strategies and analytical methods have been reported to detect the co-occurrence of mycotoxins. Recently, aptamer-modified fluorescent nanomaterials offer a great opportunity to achieve sensitive, efficient, portable, and rapid detection, overcoming the limitations and restrictions of conventional methods such as extensive detection time, limited sensitivity, complex sample pretreatment, low stability of antibodies, and relying on skilled personnel and expensive instrumentation.[13−16] For simultaneous detection, a series of the new fluorescent methods have been developed, but single excitation remains a

**Received:** August 23, 2019
**Accepted:** October 4, 2019
**Published:** October 4, 2019




DOI: 10.1021/acs.analchem.9b03880
Anal. Chem. 2019, 91, 14085−14092

big challenge.[17] Therefore, a distinct excitation wavelength is of high significance for fluorescent recognition of multiple toxins.

In the past few decades, FRET-based detection platforms, relying on the strategy of energy donor and acceptor pairs, gained considerable attention due to close proximity.[18,19] To date, a number of FRET sensors have been established to accomplish the detection of toxins with quantum dots and organic dye as an energy donor.[20,21] However, they have limitation in practical applications due to poor biodegradability and biocompatibility, photobleaching, and cytotoxicity.[22−24] As a result, the development of new effective energy acceptor and donor pairs is of high significance to overwhelm these shortcomings. Compared to conventional dye, AuNCs, with extra small size, high stability and biocompatibility, stable fluorescent emission, and size-tunable fluorescence spectra, have also been recognized to be good contenders as FRET energy donors for biosensing and bioimaging.[25−28] So, it is predicted that FRET biosensors for the concurrent toxin recognitions may be established using diverse colored AuNCs (energy donors) and, more interestingly, these AuNCs may be possibly excited by a single wavelength.

Moreover, $WS_2$ is considered as a promising candidate for the preparation of FRET-based platform due to its high fluorescent quenching ability and differential affinity toward the ssDNA.[29−32] Even though $WS_2$ nanosheet has feasible potential in FRET-based biosensors, their combination with multicolored AuNCs sensor for concurrent recognition of the numerous targets has not been explored. So there is intense demand to find out the new applications of $WS_2$ in the field of biosensing. Moreover, high fluorescent quenching ability of $WS_2$ over graphene oxide is important for the delicacy of quenching and restoration based aptasensor. Hence, stimulated by the above consequences, we consider that $WS_2$ can be used as a fluorescence quencher and recovery based biosensor for the detection of $AFB_1$ and ZEN.

In the current study, we develop a novel "turn on" FRET aptasensor for rapid, sensitive, and simultaneous recognition of $AFB_1$ and ZEN using dual-colored AuNCs (energy donors) with a single excitation wavelength. The signal probe was synthesized by conjugating AuNCs (Lp-AuNCs and BSA-AuNCs) with $AFB_1$ and ZEN aptamers, respectively, and $WS_2$ as fluorescence quencher for the quantitative analysis of mycotoxins. As compared with conventional FRET method, the developed aptasensor has distinct advantages of simultaneous detection of $AFB_1$ and ZEN based on a single excitation wavelength, photo visualization, and fluorescence quenching superiority of $WS_2$ comparable to GO. With these advantages, this study provides opportunities to construct simple, effective, and economical FRET-based platforms for multiple toxin recognition separately and simultaneously.

## EXPERIMENTAL SECTION

**Chemicals.** $HAuCl_4·3H_2O$ (hydrogen tetrachloroaurate trihydrate) and Bovine serum albumin (BSA) was received from Sigma-Aldrich (St. Louis, MO). L-Proline and NaOH were bought from Sinopharm Chemical Reagent Co. Ltd. (China). 1-Ethyl-3-(3-(dimethylamino)propyl) carbodiimide hydrochloride (EDC) and *N*-hydroxylsuccinimide sodium salt (NHS) were obtained from Aladdin Industrial Co., Ltd. (Shanghai, China). The tungsten disulfide ($WS_2$) nanosheet was purchased from Nanjing XF Nano Material Tech Co., Ltd. (Nanjing, China). The aptamer sequences of $AFB_1$ and ZEN were synthesized by Sangon Biotech Company (China). The aptamer sequences of $AFB_1$ and ZEN[33,34] are 5′-$NH_2$-AGC AGC ACA GAG GTC AGA TGG TGC TAT CAT GCG CTC AAT GGG AGA CTT TAG CTG CCC CCA CCT ATG CGT GCT ACC GTG AA-3′ and 5′-$NH_2$-TCA TCT ATC TAT GGT ACA TTA CTA TCT GTA ATG TGA TAT G-3′, respectively. All the reagents were used as received without further purification.

**Instruments.** The UV−vis absorption and F.I spectra were collected by a UV-1800 spectrophotometer (Shimadzu Co., Japan) and Hitachi F-7000 fluorescence spectrophotometer (Hitachi Co., Japan), respectively. TEM images of AuNCs and $WS_2$ were observed by JEM-2100HR (JEOL Ltd., Japan), working at 200 kV acceleration, to characterizes the morphology and size. AFM was carried out by Dimension Icon Atomic Force Microscope System (AFM, Bruker Co., Germany) to characterizes the morphology of $WS_2$

**Synthesis of Blue-Emitting (442 nm) and Red-Emitting AuNCs.** All stir bars and glassware were completely washed with aqua regia ($HNO_3$/HCl with 1:3, v/v) overnight and rinsed thoroughly with 18.2 MΩ $cm^{-1}$ water before use. Blue emitting (442 nm) and red-emitting (650 nm) gold nanoclusters were synthesized according to previous studies with a slight modification.[35−37] Briefly, for blue-emitting (442 nm) AuNCs (Lp-AuNCs), 1.0 M solution of L-proline (1.0 mL) was quickly added to 3.0 mM mL boiling solution of $HAuCl_4·3H_2O$ (4.0 mL) under vigorous stirring for 10 min. Afterward, it was cooled down at ambient temperature to obtain blue-emitting gold nanoclusters. In the typical preparation of red-emitting (650 nm) AuNCs, 10 mL of $HAuCl_4·3H_2O$ (10 mM) was added to the 10 mL BSA solution (50 mg $mL^{-1}$) under vigorous agitation at 37 °C. After 2 min, 0.5 mL of NaOH (1M) was introduced into the solution, mixed well, and incubated at 37 °C overnight. During the synthesis, BSA-AuNCs changed color from light yellow to deep brown. After overnight incubation, the solution was dialyzed, to obtained purified BSA-AuNCs, against distilled water to remove the unreacted/excess impurities. The purified BSA-AuNCs was collected and stored at 4 °C.

**Preparation of $AFB_1$-apt-Lp-AuNCs (442 nm) and ZEN-apt-BSA-AuNCs (650 nm).** For the preparation of $AFB_1$-apt-Lp-AuNCs (442 nm), 21 uL of the solution of Lp-AuNCs was added to 181 uL of PBS (pH 7.4), and NHS (0.32 mg) and EDC (0.56 mg) were added for the activation of the carboxyl group under continuous stirring for 30 min at 37 °C. After this, 20 uL of $AFB_1$ aptamer (10 uM) was added into activated Lp-AuNCs and kept at 37 °C for overnight incubation. For ZEN-apt-BSA-AuNCs (650), 3 uL of BSA-AuNCs in 197 uL of PBS was added and then NHS (0.32 mg) and EDC (0.56 mg) were added into the solution with continuous vibration at 37 °C. After 30 min, 10 uM ZEN aptamer (20 uL) was introduced into the proceeding solution and kept at 37 °C for condensation reaction.

**Sample Preparation and Measurement.** Naturally contaminated maize samples were obtained from local agriculture markets and treated according to the official method[38,39] with slight modifications. The method was concisely explained in Section 1 (S1) of the Supporting Information (SI).



DOI: 10.1021/acs.analchem.9b03880
*Anal. Chem.* 2019, 91, 14085−14092

**Scheme 1. Schematic Illustration "Switch on" of Dual-Colored AuNCs-$WS_2$FRET Biosensor for Simultaneous Detection of $AFB_1$ and ZEN Toxin**

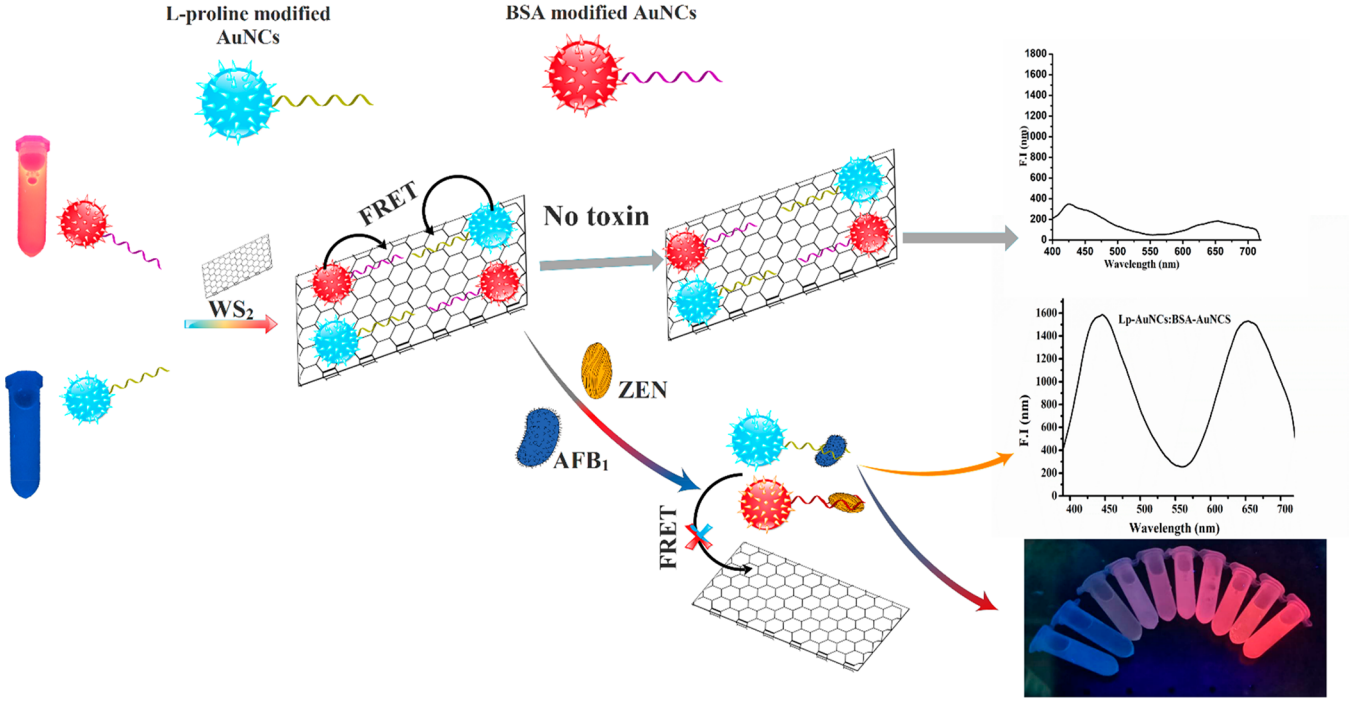


**Simultaneous Detection of $AFB_1$ and ZEN.** 100 uL of $AFB_1$-apt-Lp-AuNCs (442 nm) and 100 uL of ZEN-apt-BSA-AuNCs (650) were mixed, followed with the addition of $WS_2$ (0.30 mg $mL^{-1}$) nanosheet solution at ambient temperature for 30 min to quench the F.I. Then, the various concentration of $AFB_1$ and ZEN toxin (0.00, 0.005, 0.01, 0.05, 0.1, 0.5, 1, 10, 50, 100 ng $mL^{-1}$) were introduced into the above solution and incubated for 30 min at 37 °C to obtain recovered fluorescence spectra.

## RESULT AND DISCUSSION

**Fluorescent Detection Method.** Apt-Lp-AuNCs (blue color) and apt-BSA-AuNCs (red color) were employed with super quenching ability of $WS_2$ nanosheet for the construction of FRET-based platform from AuNCs (energy donor) to $WS_2$ (energy acceptor). Scheme 1 depicts the synthetic procedure of FRET biosensor for the simultaneous detection of $AFB_1$ and ZEN. In order to construct the sensitive platform for $AFB_1$ and ZEN detection, the AuNCs-based sensing system combined with the $WS_2$. In this study, $AFB_1$-apt-Lp-AuNCs $AFB_1$ (442 nm) and ZEN-apt-stabilized with red-colored AuNCs (650 nm) adsorbed on the $WS_2$ surface through weak van der Waals force. Due to such interaction between AuNCs and $WS_2$, the close proximity of acceptor and donor results in FRET mechanism which leads in quenching of F.I. The introduction of $AFB_1$ and ZEN weakened the interaction between aptamer and $WS_2$ due to the higher affinity between aptamer and toxins, resulted in gradual increment of F.I. Therefore, the co-occurrence of multiple toxins can be determined by monitoring the change of the restored F.I at 442 and 650 nm with a single excitation. Moreover, the quantification of multiple toxins can be measured not only by recording the recovered F.I but also by photovisualization

**Characterization of AuNCs and $WS_2$.** The Lp-AuNCs and BSA-AuNCs demonstrated light and deep brown color, which impart a blue and intense red fluorescence under a UV lamp, respectively (Figure 1A inset). To validate the potential claim of both AuNCs for simultaneous detection, the separate and mixed emission peaks were noted at single excitation of 370 nm. Lp-AuNCs and BSA-AuNCs emit at 442 and 650 nm, respectively (Figure 1A). Figure 1B exhibited the mixed emission spectra of both AuNCs that clearly differentiate them from each other and assuring the successive capability of simultaneous quantification of two toxins. Additionally, their emission spectra do not overlap, revealing their specific emission characteristics.

In order to get superior probes for simultaneous recognition in the FRET-supported platform, it is highly significant to employ a distinct excitation to minimize the background signals and greatly enhance the sensitivities averse to various excitations. Lp-AuNCs and BSA-AuNCs were excited at different excitation intensity experiments (355, 360, 365, 370, 375, 380, 385, and 390 nm). The maximum excited state for Lp-AuNCs and BSA-AuNCs is 365 and 390 nm with the emission peak of 442 and 650 nm, respectively. Though, for simultaneous recognition, a single excitation peak with maximum emission and optimized F.I was at 370 nm. Thus, 370 nm was chosen to be the optimal excitation wavelength in further experiments (Figure 1C). The concentration ratio of Lp-AuNCs and BSA-AuNCs is an important step to optimize the F.I height of both AuNCs. Figure 1D displays the influence of different concentrations of AuNCs (from 1:1 to 7:1) on the F.I peak height. The results described that the optimal peak height for simultaneous detection was achieved at 7:1 ratio for Lp-AuNCs and BSA-AuNCs, respectively.

Figure 2A–D displays the TEM images of Lp-AuNCs with the dimension of 200 ± 4 nm and 50 ± 1 nm and BSA-



DOI: 10.1021/acs.analchem.9b03880
Anal. Chem. 2019, 91, 14085−14092

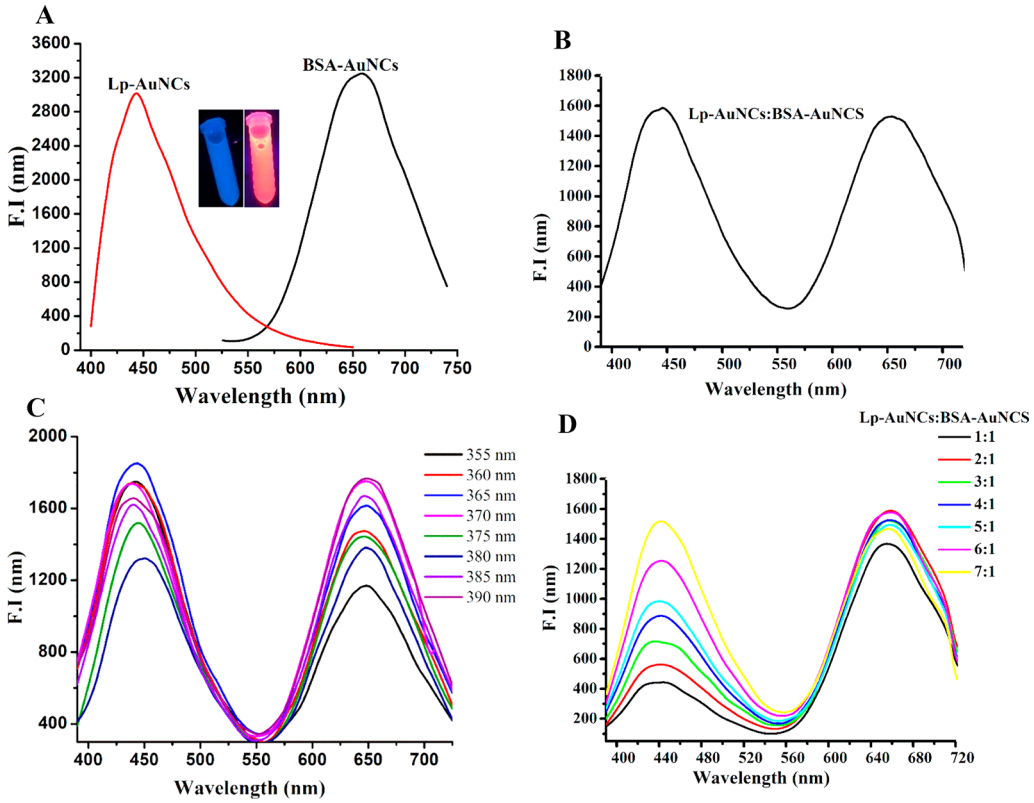


**Figure 1.** (A) Fluorescence emission spectra of Lp-AuNCs at 442 nm and BSA-AuNCs at 650. (B) Mixed emission spectra of dual-colored AuNCs in PBS. (C) The fluorescence emission spectra of AuNCs at different excitation wavelength ranged from 355 to 390 nm. (D) Different concentration ratio of Lp-AuNCs and BSA- AuNCs (1:1−7:1) for the optimized emission spectrum.

AuNCs with dimension of 100 ± 3 nm and 50 ± 2 nm. The TEM analysis clearly indicates that Lp- AuNCs and BSA-AuNCs were well dispersed, spherical shaped, and uniformly distributed with highest frequency of 1.21−3.17 nm and 1.12−2.8 nm with average diameter of 2.14 and 1.82 nm, respectively (SI Figure S1A and B). The results proved that the Lp and BSA coated AuNCs were effectively synthesized. SI Figure S2 shows the AFM of $WS_2$ nanosheet, revealing the average thickness of about ∼1.5 nm, which is consistence with the monolayers. To confirm the feasibility of the FRET assay, the emission and absorption experiments were carried out. The absorption spectrum of $WS_2$ has many similarities with $MoS_2$ and GO. As described in SI Figure S3, the emission spectrum of AuNCs and absorption spectrum of $WS_2$ overlapped very well, exhibiting the feasibility of energy transfer from AuNCs to $WS_2$.

The aptamer and AuNCs conjugation were measured by UV spectrophotometer. A strong absorbance spectrum of $AFB_1$ and ZEN aptamer was noticed at 260 nm (SI Figure S4A (curve a) and B (curve a)). After the conjugation reaction between AuNCs and aptamer, the incubation solution was filtered with 10 kDa filters at 8000 rpm. As a result, the uncombined aptamers were present into filterer. A decrease in absorbance intensity of filtrate indicates the successful conjugation of aptamer with AuNCs, as described in (SI Figure S4A (curve b) and B (curve b)).

**Optimization.** Optimization studies are important to achieve the high performance and possibility of their practical applications of the fluorescent AuNCs. The $WS_2$ nanosheet, being quencher, has a significant effect on the F.I. Therefore, the effect of different concentration of $WS_2$ nanosheet on

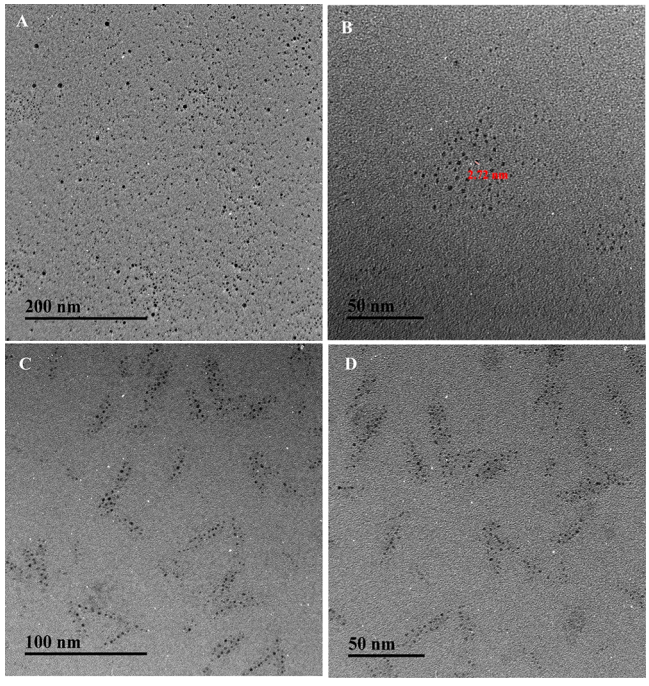


**Figure 2.** TEM images of Lp-AuNCs (442 nm) with a dimension of 200 ± 4 nm (A) and 50 ± 1 nm (B). BSA-AuNCs (650) with a dimension of 100 ± 3 nm (C) and 50 ± 2 nm (D).

aptamer modified AuNCs was studied. As described in Figure 3A, various concentration of $WS_2$ (0, 0.05, 0.10, 0.15, 0.20, 0.25, 0.30, 0.35, 0.40, 0.45, and 0.50 mg $mL^{-1}$) were used. Figure 3A (inset) also revealed the photo of fluorescence



DOI: 10.1021/acs.analchem.9b03880
Anal. Chem. 2019, 91, 14085−14092

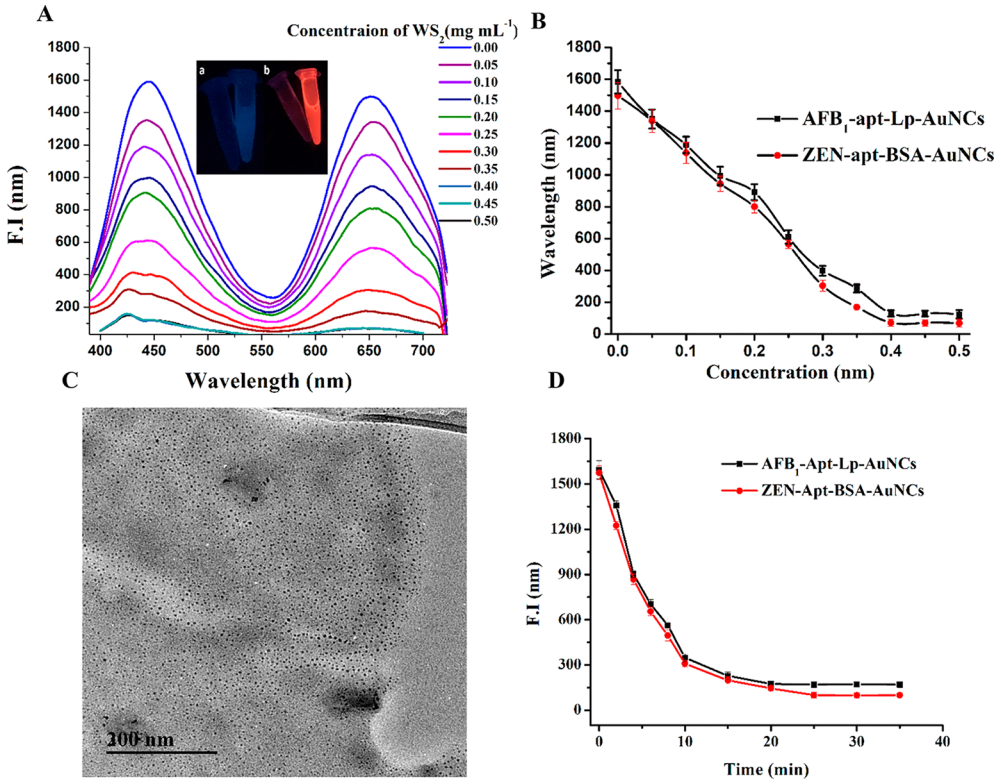


**Figure 3.** (A) Fluorescence quenching spectra of aptamer functionalized AuNCs mixtures in the presence of different concentration of $WS_2$(0, 0.05, 0.10, 0.15, 0.20, 0.25, 0.30, 0.35, 0.40, 0.45, and 0.50 mg $mL^{-1}$). (B) F.I of mixed AuNCs versus different concentration $WS_2$. (C) TEM image of mixed AuNCs mixture on the surface of $WS_2$ nanosheet. (D) Effect of different incubation time at ambient temperature (0−35 min) on the F.I for quenching mechanism.

quenching of both AuNCs in the presence of $WS_2$ (0.40 mg $mL^{-1}$). The F.I of AuNCs gradually decreased with the increasing $WS_2$ concentration from 0.05 to 0.35 mg $mL^{-1}$ and then remained stable from 0.40 to 0.50 mg $mL^{-1}$ (Figure 3B). Therefore, 0.40 mg $mL^{-1}$ was the optimized concentration for following experiments because the excessive concentration of $WS_2$ was averse to fluorescence restoration. Figure 3C also proves the presence of AuNCs on the surface of $WS_2$ demonstrated that F.I of AuNCs was quenched.

The optimized concentration of $WS_2$ nanosheet was incubated with Lp-AuNCs and BSA-AuNCs for a different time period to investigate the fluorescence quenching efficiency. As mentioned in Figure 3D, the F.I of apt-Lp-AuNCs was quenched after 25 min, whereas F.I of apt-BSA-AuNCs was quenched after 30 min at 37 °C. Considering the simultaneous detection of two toxins in the same system, 30 min was chosen as the optimized incubation time for fluorescence quenching of $WS_2$ nanosheet for further experiments.

Moreover, the interference test for $AFB_1$ and ZEN was performed using AuNCs aptasensor. First, the adjusted concentration of apt-modified Lp-AuNCs and BSA-AuNCs (7:1) was incubated with optimized $WS_2$ concentration (0.40 mg $mL^{-1}$) and then fixed concentration of $AFB_1$ and ZEN (1 ng $mL^{-1}$) was introduced separately. The whole system was incubated at 37 °C for 30 min. Afterward, the F.I was measured. As depicted in SI Figure S5, the original emission spectra of apt-modified AuNCs (curve a) was significantly quenched in the absence of $AFB_1$ and ZEN (curve b). When $AFB_1$ was separately introduced into bioassay, the F.I of the apt-modified Lp-AuNCs (at 442) was resorted (curve c), whereas the F.I of apt-modified BSA-AuNCs were almost quenched. Correspondingly, when ZEN was introduced into the sensing system, the F.I of the apt-modified BSA-AuNCs (650 nm) resorted while the other remained quenched (curve d).

The above observation clearly indicates the difference between the emission spectra of the respective probe and target while incubated with $WS_2$. It has been proven that F.I of the AuNCs bioprobes can be distinguished among two mycotoxins and can detect the $AFB_1$ and ZEN simultaneously without interfering. Therefore, the aptasensor has promising potential to detect $AFB_1$ and ZEN individually and simultaneously.

**Feasibility Validation of the Method.** The feasibility of developed aptasensor was proven by recording the emission spectra of the detection solution under various conditions as mentioned in Figure 4A. The strong F.I of apt-AuNCs (Figure 4A, curve a) was quenched by $WS_2$ nanosheet (Figure 4A, curve c). However, the F.I of sensing probe was restored after the introduction of targets to some extent due to the elimination of the weak bond between aptamer modified AuNCs and $WS_2$ that obstructs the FRET progression (Figure 4A, curve d). Furthermore, the addition of targets in the absence of $WS_2$ slightly affects the F.I of apt-AuNCs (Figure 4A, curve b) elaborating that the toxins itself do not have a striking influence on the F.I. The above consequences showed the feasibility of the aptasensor by employing FRET-based stratagem.

**Analytical Performance.** To explore the potential application, sensitivity, and general applicability of our detection system: we performed the analytical bioassay



DOI: 10.1021/acs.analchem.9b03880
Anal. Chem. 2019, 91, 14085−14092

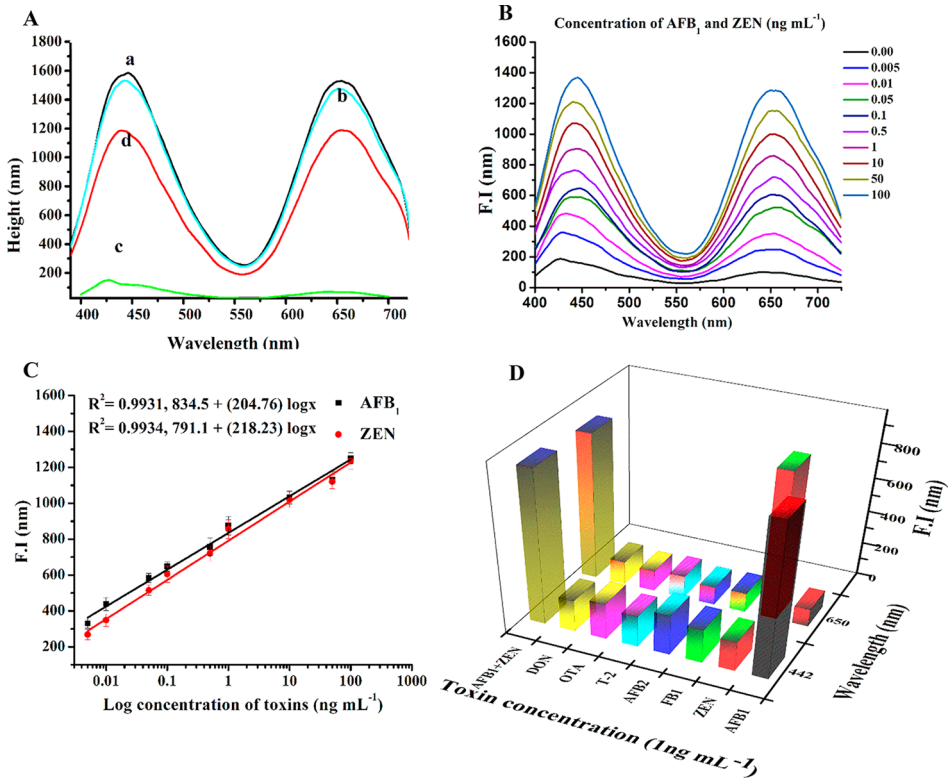


**Figure 4.** (A) F.I of AuNCs under different condition; (a) Apt-AuNCs (7:1) (b) Apt-AuNCs + toxins (c) Apt-AuNCs + $WS_2$ (0.40 mg $mL^{-1}$) (d) Apt-AuNCs + toxins ($AFB_1$; 1 ng $mL^{-1}$ + ZEN; 1 ng $mL^{-1}$) + $WS_2$(0.40 mg $mL^{-1}$). Analytical performance of bioassay. (B) F.I of the $AFB_1$-apt-AuNCs (442 nm) and ZEN-apt-AuNCs (650 nm) and $WS_2$ in the presence of different concentration of $AFB_1$ and ZEN (0.00, 0.005, 0.01, 0.05, 0.1, 0.5, 1, 10, 50, 100 ng $mL^{-1}$). (C) Linear curve for $AFB_1$ and ZEN detection. (D) Specificity of AuNCs biosensor toward $AFB_1$ and ZEN (separately and simultaneous) and others (DON, OTA, T-2, $AFB_2$ and $FB_1$) at fixed concentration (1 ng $mL^{-1}$).

**Table 1. Comparison between Our Method and Different Analytical Methods for Simultaneous Detection of $AFB_1$ and ZEN**

| toxin | method | commodity | working range | LOD | references |
|---|---|---|---|---|---|
| $AFB_1$ and ZEN | time-resolved fluorescent immune-chromatographic assay (TRFICA) | Chinese herbal medicines | 0.60−3.92 and 0.40−1.28 $\mu g\ kg^{-1}$ for $AFB_1$& ZEN, respectively. | 0.60 and 0.40 $\mu g\ kg^{-1}$, $AFB_1$ and ZEN, respectively | 40 |
| $AFB_1$ and ZEN | QB-based ICA | maize | 2−300 pg $mL^{-1}$ | 1.65 pg $mL^{-1}$ and 59.15 pg $mL^{-1}$ for $AFB_1$ and ZEN, respectively | 41 |
| $AFB_1$ and ZEN | microfluidics and array based immunoassay system | maize | 0.12−7.19 ng $mL^{-1}$ for $AFB_1$ and 1.29−16.88 ng $mL^{-1}$ for ZEN | 0.03 ng $mL^{-1}$ for $AFB_1$ and 0.58 ng $mL^{-1}$ for ZEN | 42 |
| $AFB_1$ and ZEN | TRFICA | buffer solution | 0.13−4.54 ng $mL^{-1}$ for $AFB_1$ and 0.20−2.77 ng $mL^{-1}$ for ZEN | 0.05 and 0.07 ng·$mL^{-1}$ for ZEN and $AFB_1$, respectively | 8 |
| $AFB_1$ and ZEN | TRF-aptasensor | maize | 0.001−100 ng $mL^{-1}$ | 0.51 and 0.40 pg $mL^{-1}$ for ZEN & $AFB_1$, respectively | 43 |
| $AFB_1$ and ZEN | AuNCs biosensor | maize | 0.005−100 ng $mL^{-1}$ | 0.34 pg $mL^{-1}$ and 0.53 pg $mL^{-1}$ for $AFB_1$ and ZEN, respectively | this work |

under all optimal conditions for detection of $AFB_1$ and ZEN. The concertation of the toxin is directly related to the degree of F.I recovery because more targets bind to respective apt-AuNCs and more apt-AuNCs switched away from the $WS_2$ resulting in F.I enhancement. Therefore, the different concentrations of $AFB_1$ and ZEN (0.00, 0.005, 0.01, 0.05, 0.1, 0.5, 1, 10, 50, 100 ng $mL^{-1}$) can be determined by tracking the F.I at wavelength of 442 and 650 nm (Figure 4B). It was concluded that a better relationship between the concentration of targets and F.I of $AFB_1$-apt-modified AuNCs was observed. Figure 4C shows a good linearity ($R^2$ = 0.9931, $Y$ = 834.5 + (204.76) logx) between the log concentration of $AFB_1$ (0.005−100 nm) and F.I of $AFB_1$-apt-Lp-AuNCs (at 442 nm) with detection limit (LOD) of 0.3437 pg $mL^{-1}$. Accordingly, another better linear relationship between the F.I of ZEN-BSA-AuNCs (at 650 nm) and log concentration of ZEN ranged from 0.005 to 100 nm was noted ($R^2$ = 0.9943, $Y$ = 791.1 + (218.2) logx) with LOD of 0.5384 pg $mL^{-1}$.

The LOD was calculated as

$$\mathrm{LOD} = 10^{(Y+3\mathrm{SD})-A/B}$$

$$Y = Y_{\mathrm{blank}} + 3\mathrm{SD}$$

where $Y$ blank represents the fluorescence signals of the sample without target (blank sample) and SD represents standard deviation. $A$ and $B$ are the variables obtained from least-squares root linear regression of the signal-concentration curve for variable $Y$ representing the fluorescence signal.

Additionally, a comparison between the developed aptasensor and other previously described methods for $AFB_1$ and ZEN was also presented in Table 1. As a new



DOI: 10.1021/acs.analchem.9b03880
Anal. Chem. 2019, 91, 14085−14092

sensing approach for $AFB_1$ and ZEN, the detection limit of our method is comparable to, or even better than, those of formerly stated methods.

It is notable that visual determination can also be obviously recognized by proposed bioassay. Figure 5 shows the photos

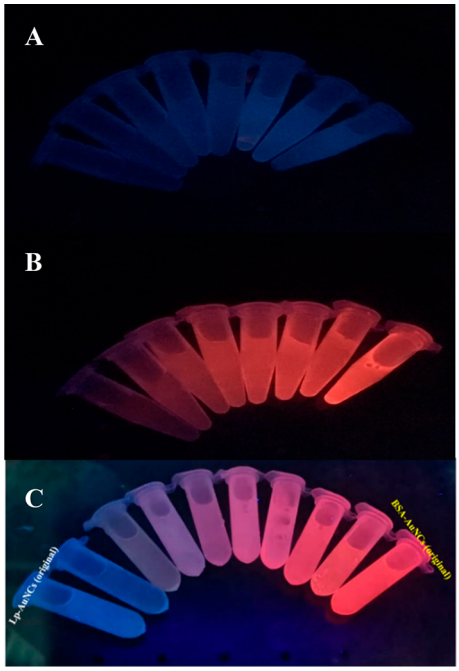


**Figure 5.** Photograph of semiquantitative determination of $AFB_1$ and ZEN separately and simultaneously, respectively (under UV light). (A) The change in F.I from quenched to recovered with different concentration of $AFB_1$ (from left to right): 0, 0.1, 0.5, 1, 5, 10, 50, 100 ng $mL^{-1}$. (B) The fluorescence quenched detection solution with different concentration of ZEN (from left to right): 0, 0.1, 0.5, 1, 5, 10, 50, 100 ng $mL^{-1}$. (C) The detection solution (quenched F.I) with the introduction of different amounts of $AFB_1$ and ZEN. The concentrations of $AFB_1$ were 100, 50, 10, 5, 1, 0.5, 0.1, and 0 ng $mL^{-1}$, and the concentrations of ZEN were 0, 0.1, 0.5, 1, 5, 10, 50, 100 ng $mL^{-1}$ (from left to right) and foremost left and right are original spectra.

of semiquantification of $AFB_1$ and ZEN separately and simultaneously, respectively (under UV light). When $AFB_1$ was introduced into the quenched fluorescent detection solution, the blue color recovered and improved rapidly with the increasing $AFB_1$ concentration (0, 0.1, 0.5, 1, 5, 10, 50, 100 ng $mL^{-1}$) (Figure 5A). Similarly, the red color of the detection solution also increased rapidly with the increasing concentration of ZEN (0, 0.1, 0.5, 1, 5, 10, 50, 100 ng $mL^{-1}$) (Figure 5B). When both $AFB_1$ and ZEN added to the detection solution, the color of the $AFB_1$-apt-Lp-AuNCs (442 nm) and ZEN-apt-BSA-AuNCs (650 nm) improved simultaneously, and also the solution displayed their mixed color (Figure 5C).

**Specificity Assay.** The competency of resisting toxins over possibly challenging species is a prerequisite for an application in food safety and control systems. So, specificity is a crucial step in the evaluation of the proposed method. In our study, the specificity of aptasensor is highly dependent on the aptamer. In order to analyze the selectivity and sensitivity of developed biosensor, the specificity of the biosensor to $AFB_1$ and ZEN over some possible toxins (DON, OTA, T-2, $AFB_2$, $FB_1$) was investigated under the same conditions and procedure as the fixed concentration of 1 ng $mL^{-1}$ for all mycotoxins. As mentioned in Figure 4D, the influences on the restored F.I of interference was negligible. In contrast, a strong influence in the F.I was observed when $AFB_1$ and ZEN were present in a detection solution separately/simultaneously, demonstrating the excellent selectivity of the assay for $AFB_1$ and ZEN.

**Analytical Applications.** To further to explore the potential and practical application, effectiveness, and accuracy of the developed method, tests were performed to measure the recoveries percentage of $AFB_1$ and ZEN in maize samples. The maize samples were spiked with different concentrations (1, 10, 50, 100, 200 ng $mL^{-1}$) of toxins. The recovery ratios of $AFB_1$ in maize samples ranged from 98% to 118.73%, and those for ZEN in maize sample were between 94.36% and 110.4%. The results are summarized in SI Table S1. Moreover, the results of the proposed method were also compared with the standard ELISA method to confirm the accuracy and consistency of the developed method. The results, summarized in SI Figure S6, disclosed that these two detection methods are highly correlated with each other. There is no significant difference between developed and standard ELISA method for the recognition and quantification of $AFB_1$ and ZEN in maize. These findings demonstrate that the developed assay could be applied for the quantitative recognition and quantification of toxins in agriculture products.

## CONCLUSION

In summary, we hereby synthesized a "turn on" FRET biosensor based on dual-color AuNCs, as an output signal, for simultaneous detection of multiple toxin targets. For the first time, we combined the unique fluorescent quenching property of $WS_2$ (energy acceptor) with dual-colored AuNCs (energy donor). Without spectra overlapping, the two distinct fluorescence signals can be simultaneously realized by a single excitation wavelength, and the concurrent detection of $AFB_1$ and ZEN can be easily monitored. Moreover, photo visualization can be used for the semiquantitative determination of $AFB_1$ and ZEN. The present aptasensor provide an accurate and reliable approach for simultaneous recognition. It is expected that the proposed aptasensor may greatly contribute to developing novel detection approaches and expands its application in various fields.

## ASSOCIATED CONTENT

### Supporting Information

The Supporting Information is available free of charge on the ACS Publications website at DOI: 10.1021/acs.analchem.9b03880.

Additional information as noted in the text (PDF)

## AUTHOR INFORMATION

### Corresponding Author

*E-mail: wangzp1974@163.com; wangzp@jiangnan.edu.cn.

### ORCID

Muhammad Waheed Iqbal: 0000-0003-3386-7973

Zhouping Wang: 0000-0002-3868-8125

### Notes

The authors declare no competing financial interest.



DOI: 10.1021/acs.analchem.9b03880
Anal. Chem. 2019, 91, 14085−14092

## ■ ACKNOWLEDGMENTS

This work was partly funded by the National Natural Science Foundation of China (31871881), Jiangsu Agriculture Science and Technology Innovation Fund (JASTIF) (CX (18)2025), Zhangjiagang Science and Technology Support Plan (Social development) (ZKS 1803), S&T Support Program of Jiangsu Province (BE2017623), the National First-class Discipline Program of Food Science and Technology (JUFSTR20180303), and the Distinguished Professor Program of Jiangsu Province.

## ■ REFERENCES

(1) Zhang, D.; You, H.; Yuan, L.; Hao, R.; Li, T.; Fang, J. *Anal. Chem.* **2019**, *91* (7), 4687−4695.
(2) Wielogorska, E.; Mooney, M.; Eskola, M.; Ezekiel, C. N.; Stranska, M.; Krska, R.; Elliott, C. *J. Agric. Food Chem.* **2019**, *67* (7), 2052−2060.
(3) Ye, Y.; Guo, H.; Sun, X. *Biosens. Bioelectron.* **2019**, *126*, 389−404.
(4) Lv, M.; Liu, Y.; Geng, J.; Kou, X.; Xin, Z.; Yang, D. *Biosens. Bioelectron.* **2018**, *106*, 122−128.
(5) Cao, Y.; Feng, T.; Xu, J.; Xue, C. *Biosens. Bioelectron.* **2019**, *141*, 111447.
(6) Goud, K. Y.; Kailasa, S. K.; Kumar, V.; Tsang, Y. F.; Lee, S. E.; Gobi, K. V.; Kim, K.-H. *Biosens. Bioelectron.* **2018**, *121*, 205−222.
(7) Alhamoud, Y.; Yang, D.; Fiati Kenston, S. S.; Liu, G.; Liu, L.; Zhou, H.; Ahmed, F.; Zhao, J. *Biosens. Bioelectron.* **2019**, *141*, 111418.
(8) Tang, X.; Li, P.; Zhang, Q.; Zhang, Z.; Zhang, W.; Jiang, J. *Anal. Chem.* **2017**, *89* (21), 11520−11528.
(9) Ji, X.; Yu, C.; Wen, Y.; Chen, J.; Yu, Y.; Zhang, C.; Gao, R.; Mu, X.; He, J. *Biosens. Bioelectron.* **2019**, *129*, 139−146.
(10) Xia, S.; Zhu, P.; Pi, F.; Zhang, Y.; Li, Y.; Wang, J.; Sun, X. *Biosens. Bioelectron.* **2017**, *97*, 345−351.
(11) Ji, W.; Zhang, Z.; Tian, Y.; Yang, Z.; Cao, Z.; Zhang, L.; Qi, Y.; Chang, J.; Zhang, S.; Wang, H. *ACS Appl. Mater. Interfaces* **2019**, *11* (8), 8584−8590.
(12) Wei, T.; Ren, P.; Huang, L.; Ouyang, Z.; Wang, Z.; Kong, X.; Li, T.; Yin, Y.; Wu, Y.; He, Q. *Food Chem.* **2019**, *300*, 125176.
(13) Niazi, S.; Khan, I. M.; Yan, L.; Khan, M. I.; Mohsin, A.; Duan, N.; Wu, S.; Wang, Z. *Anal. Bioanal. Chem.* **2019**, *411* (7), 1453−1465.
(14) Niazi, S.; Wang, X.; Pasha, I.; Khan, I. M.; Zhao, S.; Shoaib, M.; Wu, S.; Wang, Z. *Talanta* **2018**, *186*, 97−103.
(15) Khan, I. M.; Zhao, S.; Niazi, S.; Mohsin, A.; Shoaib, M.; Duan, N.; Wu, S.; Wang, Z. *Sens. Actuators, B* **2018**, *277*, 328−335.
(16) Wang, N.; Dai, H.; Sai, L.; Ma, H.; Lin, M. *Biosens. Bioelectron.* **2019**, *126*, 529−534.
(17) Situ, B.; Gao, M.; He, X.; Li, S.; He, B.; Guo, F.; Kang, C.; Liu, S.; Yang, L.; Jiang, M.; Hu, Y.; Tang, B. Z.; Zheng, L. *Mater. Horiz.* **2019**, *6* (3), 546−553.
(18) Youn, H.; Lee, K.; Her, J.; Jeon, J.; Mok, J.; So, J.-i.; Shin, S.; Ban, C. *Sci. Rep.* **2019**, *9* (1), 7659.
(19) Zhang, G.; Ji, R.; Kong, X.; Ning, F.; Liu, A.; Cui, J.; Ge, Y. *RSC Adv.* **2019**, *9* (2), 1147−1150.
(20) Guo, P.; Yang, W.; Hu, H.; Wang, Y.; Li, P. *Anal. Bioanal. Chem.* **2019**, *411* (12), 2607−2617.
(21) Gao, J.; Chen, Z.; Mao, L.; Zhang, W.; Wen, W.; Zhang, X.; Wang, S. *Talanta* **2019**, *199*, 178−183.
(22) Herrera, V.; Hsu, S.-C. J.; Rahim, M. K.; Chen, C.; Nguyen, L.; Liu, W. F.; Haun, J. B. *Analyst* **2019**, *144* (3), 980−989.
(23) Carrillo-Carrion, C.; Bocanegra, A. I.; Arnaiz, B.; Feliu, N.; Zhu, D.; Parak, W. J. *ACS Nano* **2019**, *13* (4), 4631−4639.
(24) Cardenas-Morcoso, D.; Gualdroón-Reyes, A. s. F.; Ferreira Vitoreti, A. B.; García-Tecedor, M.; Yoon, S. J.; Solis de la Fuente, M.; Mora-Seroó, I. n.; Gimenez, S. *J. Phys. Chem. Lett.* **2019**, *10* (3), 630−636.
(25) Sokołowska, K.; Malola, S.; Lahtinen, M.; Saarnio, V.; Permi, P.; Koskinen, K.; Jalasvuori, M.; Haäkkinen, H.; Lehtovaara, L.; Lahtinen, T. *J. Phys. Chem. C* **2019**, *123* (4), 2602−2612.
(26) Fu, Y.; Jin, H.; Bu, X.; Gui, R. *J. Agric. Food Chem.* **2018**, *66* (37), 9819−9827.
(27) Zhao, Q.; Zhou, C.; Yang, Q.; Chu, Z.; Jia, N. *Microchim. Acta* **2019**, *186* (5), 294.
(28) Jia, T.-T.; Yang, G.; Mo, S.-J.; Wang, Z.-Y.; Li, B.-J.; Ma, W.; Guo, Y.-X.; Chen, X.; Zhao, X.; Liu, J.-Q.; Zang, S.-Q. *ACS Nano* **2019**, *13* (7), 8320−8328.
(29) Li, A.; Zhang, J.; Qiu, J.; Zhao, Z.; Wang, C.; Zhao, C.; Liu, H. *Talanta* **2017**, *163*, 78−84.
(30) Sui, C.; Wang, T.; Zhou, Y.; Yin, H.; Meng, X.; Zhang, S.; Waterhouse, G. I.; Xu, Q.; Zhuge, Y.; Ai, S. *Biosens. Bioelectron.* **2019**, *127*, 38−44.
(31) Yang, J.; Gao, L.; Peng, C.; Zhang, W. *RSC Adv.* **2019**, *9* (17), 9613−9619.
(32) Liu, B.; Wu, T.; Huang, Z.; Liu, Y.; Liu, J. *Angew. Chem.* **2019**, *131* (7), 2131−2135.
(33) Ma, X.; Wang, W.; Chen, X.; Xia, Y.; Wu, S.; Duan, N.; Wang, Z. *Eur. Food Res. Technol.* **2014**, *238* (6), 919−925.
(34) Chen, X.; Huang, Y.; Duan, N.; Wu, S.; Ma, X.; Xia, Y.; Zhu, C.; Jiang, Y.; Wang, Z. *Anal. Bioanal. Chem.* **2013**, *405* (20), 6573−6581.
(35) Xu, S.; Nie, Y.; Jiang, L.; Wang, J.; Xu, G.; Wang, W.; Luo, X. *Anal. Chem.* **2018**, *90* (6), 4039−4045.
(36) Hu, X. L.; Wu, X. M.; Fang, X.; Li, Z. J.; Wang, G. L. *Biosens. Bioelectron.* **2016**, *77*, 666−672.
(37) Xiong, J.; Xu, K.; Hou, X.; Wu, P. *Anal. Chem.* **2019**.*916141*
(38) LS/T6111−2015. Inspection of grain and oils. Detection of Aflatoxin B1 in grain. Rapid quantitative method of colloidal gold technique. In *Standardization Administration of the People's Republic of China*, 2015.
(39) GB5009.209−2016. *National Food Safety Standard Determination of Zearalenone in Foods, 5009, National Standards of the People's Republic of China*, 2016.
(40) Sun, S.; Zheng, P.; Zhao, S.; Liu, H.; Wang, Z.; Peng, T.; Wang, J.; Yao, K.; Wang, S.; Zeng, Y.; Jiang, H. *Food Addit. Contam., Part A* **2018**, *35* (12), 2434−2442.
(41) Shao, Y.; Duan, H.; Guo, L.; Leng, Y.; Lai, W.; Xiong, Y. *Anal. Chim. Acta* **2018**, *1025*, 163−171.
(42) Chen, Y.; Meng, X.; Zhu, Y.; Shen, M.; Lu, Y.; Cheng, J.; Xu, Y. *Talanta* **2018**, *186*, 299−305.
(43) Niazi, S.; Khan, I. M.; Yu, Y.; Pasha, I.; Shoaib, M.; Mohsin, A.; Mushtaq, B. S.; Akhtar, W.; Wang, Z. *Microchim. Acta* **2019**, *186* (8), 575.



DOI: 10.1021/acs.analchem.9b03880
*Anal. Chem.* 2019, 91, 14085−14092